Multidimensional non-linear laser imaging of Basal Cell Carcinoma

R. Cicchi[1], D. Massi[2], S. Sestini[3], P. Carli[3], V. De Giorgi[3], T. Lotti[3], and F. S. Pavone[1]

[1]LENS and Department of Physics, University of Florence,Via Nello Carrara 1, 50019, Sesto Fiorentino, Italy
[2]Department of Human Pathology and Oncology, University of Florence,Viale Morgagni 58, 50134, Florence, Italy
[3]Department of Dermatology, University of Florence,Via della Pergola 62, 50121, Florence, Italy
Corresponding author: rikka@lens.unifi.it

Abstract: We have used a multidimensional non-linear laser imaging approach to visualize *ex-vivo* samples of basal cell carcinoma (BCC). A combination of several non-linear laser imaging techniques involving fluorescence lifetime, multispectral two-photon and second-harmonic generation imaging has been used to image different skin layers. This approach has elucidated some morphological (supported by histopathological images), biochemical, and physiochemical differences of the healthy samples with respect to BCC ones. In particular, in comparison with normal skin, BCC showed a blue-shifted fluorescence emission, a higher fluorescence response at 800 nm excitation wavelength and a slightly longer mean fluorescence lifetime. Finally, the use of aminolevulinic acid as a contrast agent has been demonstrated to increase the constrast in tumor border detection. The results obtained provide further support for *in-vivo* non-invasive imaging of Basal Cell Carcinoma.

OCIS codes: (180.5810) Scanning microscopy; (170.6510) Spectroscopy; (110.4190) Multiple imaging;

References and links

1. W. Denk, J. H. Strickler and W. W. Webb, "Two-photon laser scanning fluorescence microscope," Science **248**, 73-76 (1990).
2. W. R. Zipfel, R. M. Williams and W. W. Webb, "Nonlinear magic: multiphoton microscopy in the biosciences," Nat. Biotechnol. **21**, 1369-1377 (2003).
3. A. Zoumi, A. Yeh and B. J. Tromberg, "Imaging cells and extracellular matrix in vivo by using second harmonic generation and two-photon excited fluorescence," Proc. Natl. Acad. Sci. USA **99**, 11014-11019 (2002).
4. W. R. Zipfel, R. M. Williams, R. Christie, A. Y. Nikitin, B. T. Hyman and W. W. Webb, "Live tissue intrinsic emission microscopy using multiphoton-excited native fluorescence and second harmonic generation," Proc. Natl. Acad. Sci. USA **100**, 7075-7080 (2003).
5. B. R. Masters, P. T. C. So and E. Gratton, "Optical biopsy of in vivo human skin: multi-photon excitation microscopy," Lasers Med. Sci. **13**, 196-203 (1998).
6. P. T. C. So, H. Kim and I. E. Kochevar, "Two-Photon deep tissue ex vivo imaging of mouse dermal and subcutaneous structures," Opt. Express **3**, 339-351 (1998).
7. J. C. Malone, A. F. Hood, T. Conley, J. Nürnberger, L. A. Baldridge, J. L. Clendenon, K. W. Dunn and C. L. Phillips, "Three-dimensional imaging of human skin and mucosa by two-photon laser scanning microscopy," J. Cutan. Pathol. **29**, 453-458 (2002).
8. B. R. Masters and P. T. C. So, "Confocal microscopy and multi-photon excitation microscopy of human skin in vivo," Opt. Express **8**, 2-9 (2001).
9. K. König and I. Riemann, "High-resolution multiphoton tomography of human skin with subcellular spatial resolution and picosecond time resolution," J. Biomed. Opt. **8**(3), 432-439 (2003).
10. L. Moreaux, O. Sandre, S. Charpak, M. Blanchard-Desce and J. Mertz, "Coherent scattering in multi-harmonic light microscopy," Biophys. J. **80**(3), 1568-1574 (2001).
11. P. J. Campagnola and L. M. Loew, "Second-harmonic imaging microscopy for visualizing biomolecular arrays in cells, tissues and organisms," Nat. Biotechnol. **21**, 1356-1360 (2003).
12. P. J. Campagnola, A. C. Millard, M. Terasaki, P. E. Hoppe, C. J. Malone and W. A. Mohler, "Three-dimensional high-resolution second-harmonic generation imaging of endogenous structural proteins in biological tissues," Biophys. J. **81**, 493-508 (2002).
13. S. Roth and I. Freund, "Second harmonic generation in collagen," J. Chem. Phys. **70**, 1637-1643 (1979).

#85395 - $15.00 USD Received 17 Jul 2007; revised 24 Jul 2007; accepted 24 Jul 2007; published 26 Jul 2007

14. K. König, K. Schenke-Layland, I. Riemann and U. A. Stock, "Multiphoton autofluorescence imaging of intratissue elastic fibers," Biomaterials **26**, 495-500 (2005).
15. R. M. Williams, W. R. Zipfel and W. W. Webb, "Interpreting second-harmonic generation images of collagen I fibrils," Biophys. J. **88**, 1377-1386 (2005).
16. P. Stoller, K. M. Reiser, P. M. Celliers and A. M. Rubenchik, "Polarization-modulated second harmonic generation in collagen," Biophys. J. **82**, 3330-3342 (2002).
17. T. Yasui, Y. Tohno and T. Araki, "Characterization of collagen orientation in human dermis by two-dimensional second-harmonic-generation polarimetry," J. Biomed. Opt. **9**(2), 259-264 (2004).
18. Y. Sun, W. L. Chen, S. J. Lin, S. H. Jee, Y. F. Chen, L. C. Lin, P. T. C. So and C. Y. Dong, "Investigating mechanisms of collagen thermal denaturation by high resolution second-harmonic generation imaging," Biophys. J. **91**, 2620-2625 (2006).
19. M. Han, G. Giese and J. F. Bille, "Second harmonic generation imaging of collagen fibrils in cornea and sclera," Opt. Express **13**, 5791-5797 (2005).
20. E. Brown, T. McKee, E. DiTomaso, A. Pluen, B. Seed, Y. Boucher and R. K. Jain, "Dynamic imaging of collagen and its modulation in tumors in vivo using second-harmonic generation," Nat. Med. **9**, 796-800 (2003).
21. S. J. Lin, S. H. Jee, C. J. Kuo, R. J. Wu, W. C. Lin, J. S. Chen, Y. H. Liao, C. J. Hsu, T. F. Tsai, Y. F. Chen and C. Y. Dong, "Discrimination of basal cell carcinoma from normal dermal stroma by quantitative multiphoton imaging," Opt. Lett. **31**, 2756-2758 (2006).
22. P. P. Provenzano, K. W. Eliceiri, J. M. Campbell, D. R. Inman, J. G. White and P. J. Keely, "Collagen reorganization at the tumor-stromal interface facilitates local invasion," BMC Med. **4**(1), 38 (2006).
23. S. J. Lin, R. J. Wu, H. Y. Tan, W. Lo, W. C. Lin, T. H. Young, C. J. Hsu, J. S. Chen, S. H. Jee and C. Y. Dong, "Evaluating cutaneous photoaging by use of multiphoton fluorescence and second-harmonic generation microscopy," Opt. Lett. **17**, 2275-2277 (2005).
24. M. J. Koehler, K. König, P. Elsner, R. Bückle and M. Kaatz, "In vivo assessment of human skin aging by multiphoton laser scanning tomography," Opt. Lett. **19**, 2879-2881 (2006).
25. P. J. Tadrous, "Methods for imaging the structure and function of living tissues and cells: 2. Fluorescence lifetime imaging," J. Pathol. **191**, 229-234 (2000).
26. P. J. Tadrous, J. Siegel, P. M. W. French, S. Shousha, E. N. Lalani and G. W. H. Stamp, "Fluorescence lifetime imaging of unstained tissues: early results in human breast cancer," J. Pathol. **199**, 309-317 (2003).
27. Y. Chen and A. Periasamy, "Characterization of two-photon excitation fluorescence lifetime imaging microscopy for protein localization," Microsc. Res. Tech. **63**(1), 72-80 (2004).
28. S. Y. Breusegem, M. Levi and N. P. Barry, "Fluorescence correlation spectroscopy and fluorescence lifetime imaging microscopy," Nephron. Exp. Nephrol. **103**(2), e41-e49 (2006).
29. K. M. Hanson, M. J. Behne, N. P. Barry, T. M. Mauro, E. Gratton and R. M. Clegg, "Two-photon fluorescence lifetime imaging of the skin stratum corneum pH gradient," Biophys. J. **83**, 1682-1690 (2002).
30. A. M. Pena, M. Strupler, T. Boulesteix and M. C. Shanne-Klein, "Spectroscopic analysis of keratin endogenous signal for skin multiphoton microscopy," Opt. Express **13**, 6268-6274 (2005).
31. L. H. Laiho, S. Pelet, T. M. Hancewicz, P. D. Kaplan and P. T. C. So, "Two-photon 3-D mapping of ex vivo human skin endogenous fluorescence species based on fluorescence emission spectra," J. Biomed. Opt. **10**(2), 024016 (2005).
32. J. Chen, S. Zhuo, T. Luo, X. Jiang and J. Zhao, "Spectral characteristics of autofluorescence and second harmonic generation from ex vivo human skin induced by femtosecond laser and visible lasers," *Scanning* **28**(6), 319-326 (2006).
33. S. Gonzalez and Z. Tannous, "Real-time in vivo confocal reflectance microscopy of basal cell carcinoma," J. Am. Acad. Dermatol. **47**, 869-874 (2002).
34. D. E. Marra, A. Torres, C. F: Schanbacher and S. Gonzalez, "Detection of residual basal cell carcinoma by in vivo confocal microscopy," Dermatol. Surg. **31**, 538-541 (2005).
35. M. B. Ericson, J. Uhre, C. Strandeberg, B. Stenquist, O. Larko, A. M. Wennberg and A. Rosen, "Bispectral fluorescence imaging combined with texture analysis and linear discrimination for correlation with histopathologic extent of basal cell carcinoma," J. Biomed. Opt. **10**(3), 034009 (2005).
36. S. Andersson-Engels, G. Canti, R. Cubeddu, C. Eker, C. af Klinteberg, A. Pifferi, K. Svanberg, S. Svanberg, P. Taroni, G. Valentini and I. Wang, "Preliminary evaluation of two fluorescence imaging methods for the detection and the delineation of basal cell carcinomas of the skin," Lasers Surg. Med. **26**(1), 76-82 (2000).
37. J. E. Blume and A. R. Oseroff, "Aminolevulinic acid photodynamic therapy for skin cancers," Dermatol. Clin. **25**(1), 5-14 (2007).
38. J. C. Kennedy, R. H. Pottier and D. C. Pross, "Photodynamic therapy with endogenous protoporphyrine IX: Basic principles and present clinical experience," J. Photochem. Photobiol. B **6**, 143-148 (1990).
39. M. Kress, T. Meier, R. Steiner, F. Dolp, R. Erdmann, U. Ortmann and A. Rück, "Time-resolved microspectrofluorometry and fluorescence lifetime imaging of photosensitizers using picosecond pulsed diode lasers in laser scanning microscopes," J. Biomed. Opt. **8**(1), 26-32 (2003).
40. J. R. Lackowicz, H. Szmacinski, K. Nowaczyk, K. W. Berndt and M. Johnson, "Fluorescence lifetime imaging," Ann. Biochem. **202**: 316-330 (1992).
41. M. C. Skala, K. M. Riching, D. K. Bird, A. Gendron-Fitzpatrick, J. Eickhoff, K. W. Eliceiri, P. J. Keely and N. Ramanujam, "In vivo multiphoton fluorescence lifetime imaging of protein-bound and free nicotinamide adenine dinucleotide in normal and precancerous epithelia," J. Biomed. Opt. **12**(2), 024014 (2007).
42. T. Mitschele, B. Diesel, M. Friedrich, V. Meineke, R. M. Maas, B. C. Gärtner, J. Kamradt, E. Meese, W. Tilgen and J. Reichrath, "Analysis of the vitamin D system in basal cell carcinomas (BCCs)," Lab. Invest. **84**, 693-702 (2004).

#85395 - $15.00 USD Received 17 Jul 2007; revised 24 Jul 2007; accepted 24 Jul 2007; published 26 Jul 2007

43. D. D. Bikle, Y. Oda and Z. Xie, "Vitamin D and skin cancer: A problem in gene regulation," J. Steroid. Biochem. Mol. Biol. **97**, 83-91 (2005).

1. Introduction

Non-linear laser microscopy imaging represents an important tool for the characterization of many skin pathologies. The complexity in the specific assessment of a skin tumor, related to morpho-functional characteristics (i.e. specificity of protein abundances and morphological distributions in different skin layers), requires a multidimensional analysis.

Two-photon excitation (TPE) fluorescence microscopy is a high-resolution laser imaging technique enabling deep optical tissue imaging [1,2]. Because both cells and extracellular matrix intrinsically contain a variety of fluorescent molecules (NADH, tryptophan, keratins, melanin, elastin, cholecalciferol and others), biological tissues can be imaged by TPE microscopy without any exogenous probe [3,4]. TPE microscopy has already been successfully used as a powerful technique in skin imaging and optical biopsy by means of a morphological characterization [5-9]. Additional morphological information can be provided by second harmonic generation (SHG) microscopy, which can be combined with TPE microscopy using the same laser source. SHG has already been largely used for imaging non-centrosymmetric molecules inside cells [10,11] and tissues [12-14]. Collagen fibers produce a high second harmonic signal [13] and can be imaged inside skin dermis with SHG microscopy [4,15]. Recently, SHG was also used for investigating collagen fibers orientation and their structural changes in healthy tissues as human dermis [16-18] or cornea [19] and in the tumor microenvironement [20-22]. Combined TPE-SHG microscopy has been applied to skin physiology and pathology, and specifically to the study of normal skin [5-9,18], skin photoaging [23,24], cutaneous psoriasis [9], and certain skin tumors, including BCC [20,21], and malignant melanoma [9].

Fluorescence lifetime imaging microscopy (FLIM) is an additional non-invasive microscopy technique enabling the identification of endogenous fluorescent molecules and their surrounding medium by measuring the decay rate of fluorescence emission [25,26]. FLIM is useful to study protein localization [27] and fluorescent molecular environment [28]. TPE-FLIM has been previously applied to the study of the fluorescent properties of normal skin [24,29] and has been demonstrated as an important tool to characterize skin layers specificity [9].

Finally, multispectral (MTPE) tissue imaging can also be performed by measuring the two photon emission spectra of different tissue proteins. Those techniques offer functional information about the relative quantities of fluorescent molecules, which correlate with tissue structure in physiological and pathological states [30-32].

Regarding BCC imaging, some work has been done with linear laser techniques (reflectance confocal [33,34], single photon fluorescence [35], one photon lifetime [36]). Confocal reflectance microscopy is able to obtain a substantial penetration depth (100-200μm) and morphological information, while single photon fluorescence and lifetime provide more functional (chemical) information but with a much reduced penetration depth (surface detection).

Non-linear laser imaging has the advantage of performing both morphological and functional analysis with a good penetration depth (200 μm). S.Lin et al. [20] have recently reported TPE and SHG imaging of thin cross section slices (7-10mm thickness) of *ex-vivo* BCC samples. In that work the authors measured the TPE/SHG signal ratio in different skin regions, as the healthy dermis, basal cell carcinoma and tumor stroma surroundings.

In this work, we have used a different approach for the BCC non-linear laser imaging with respect to Lin et al. [20]. As a first difference we have used both thick perpendicular and en face skin bioptic samples (about $1cm^3$ sample), in order to provide with this work further support for *in-vivo* imaging.

#85395 - $15.00 USD Received 17 Jul 2007; revised 24 Jul 2007; accepted 24 Jul 2007; published 26 Jul 2007

Furthermore, we have perfomed FLIM and MTPE measurements, in addition to TPE and SHG, in order to detect not only morphological differences between healthy skin and BCC, but also spectroscopic (chemical) ones.

Finally, we have used the Aminolevulinic Acid (ALA) as a tumor marker. ALA is a compound commonly used in photodynamic therapy [37] of skin cancer. When topically applied to the skin lesion, ALA causes the selective accumulation of protoporphyrine IX (PpIX) inside skin tumor tissue, with high tumor to surrounding medium ratio [38]. ALA has already been used as a contrast agent for BCC in fluorescence microscopy [35] and one-photon lifetime imaging [36], but its effectiveness in TPE microscopy of skin has not been reported yet. Measurements of BCC and healthy skin samples where done in this case by using TPE and FLIM detections in order to reveal the contrast enhancement of the tumor border by ALA labeling.

2. Materials and methods

2.1 Experimental setup

2.1.1 Custom-made optical microscope

The experimental setup is constituted by a custom-made upright microscope, built with the collaboration of the university workshop, able to perform TPE fluorescence microscopy, SHG microscopy, conventional wide-field microscopy and FLIM with spectrally-resolved detection. All the microscope optics are fixed onto a custom vertical honeycomb steel breadboard 60 × 90 cm, 070BH0450 (Melles-Griot, Rochester, NY, US), mounted by two square brackets onto an anti-vibrating optical table 100 × 200 cm (TMC, Peabody, MA, US). For the wide-field subsystem, the light source is a metallic ring with six superluminescent diodes placed around the objective lens. The image of the investigated sample is projected onto a color CCD camera COOLPIX 4700 (Nikon, Tokyo, Japan) using a tilting mirror.

2.1.2 Two-photon excitation fluorescence detection

In the TPE fluorescence subsystem a mode-locked Ti:Sapphire laser CHAMELEON (Coherent Inc, Santa Clara, CA, US) provides the pulsed excitation light, tunable in wavelength in the 705-980 nm range. The laser light beam path includes a collimating telescope, a half-wavelength waveplate ($\lambda/2$) coupled with a calcite polarizing beam splitter (PBS) for laser power adjustment, and an electronic shutter. The scanning head comprises two galvanometer mirrors VM500 (GSI Lumonics, Munich, Germany), optically coupled by a pair of spherical mirrors (Casix, Fuzhou, China). A scanning lens and microscope tube lens expand the beam to a dimension of 1 cm, before it is focused by the objective lens XLUM 20X, NA 0.9, WD 2 mm (Olympus Co., Japan). A piezoelectric stage PIFOC P-721 (Physik Instrumente GmbH, Karlsruhe, Germany) allows axial displacements of the objective up to 100 μm with 1 nm resolution.

Fluorescence light is separated from the laser optical path by a dichroic filter 685DCXRU (Chroma Technology Corporation, Rockingham, VT, US) positioned as close as possible to the objective lens (non de-scanning mode), before being focused by a lens and collected onto a photomultiplier detector H7710-13 (Hamamatsu Photonics, Hamamatsu City, Japan) interfaced through custom electronics with an acquisition board PCI-MIO-16E (National Instruments, Austin, TX, US). A cut-off filter E700SP-2P (Chroma Technology Corporation, Rockingham, VT, US) eliminates reflected laser light. Second harmonic light is detected by inserting a narrow band optical filter HQ420/10 (Chroma Technology Corporation, Rockingham, VT, US) in the fluorescence path.

2.1.3 Fluorescence lifetime, spectral lifetime and multispectral two photon detections

The FLIM detection system includes a couple of lenses, constituting a telescope, and an objective lens Plan 10X, 0.25 NA (Nikon, Tokyo, Japan), which couples the fluorescence light into a multimode optical fiber, directly connected to the detection system. The detector

#85395 - $15.00 USD Received 17 Jul 2007; revised 24 Jul 2007; accepted 24 Jul 2007; published 26 Jul 2007

PML-Spec (Becker-Hickl GmbH, Berlin, Germany) is constituted by a diffraction grating with 600 lines/mm and a 16-channels multi-anode photomultiplier strip with 200 ps FWHM pulses, allowing spectrally-resolved (13 nm resolution) detection of fluorescence light (MTPE). Acquisition and control are performed using a PC and two synchronized I/O boards, a PCI-MIO-16E, controlling the movements of the scanning mirrors, and a SPC-730 (Becker-Hickl GmbH, Berlin, Germany), dedicated to time-resolved single photon counting measurements. The output settings are controlled by a custom-made software developed in LabView environment. Visualization of the acquired images is accomplished with a dedicated software SPCM 1.1 (Becker-Hickl GmbH, Berlin, Germany) that also allows changes in the photon counting board settings. A removable mirror allows switching between the two detection systems.

2.2 Patients

This study included 25 BCC samples (16 nodular, 6 superficial and 3 sclerodermiform/morphea-like) surgically removed from 25 patients (13 males and 12 females; age range 43-67 years). Imaging was performed after obtaining a written consent from all the patients. The nodular lesions had a diameter less than 1 cm, six of them were partially pigmented. In all cases, the clinical diagnosis was confirmed by conventional histopathological examination. In four cases (nodular type) we topically applied 2 ml of 20% ALA (Methylaminolevulined 160 mg/g-Metvix® cream) on the lesions. The patients entered the surgical room at least 3-4 hours after application. Each lesion was excised with at least 2-3 mm healthy skin margins. Upon excision, the skin specimen was halved in two parts, one submitted to conventional histology and the other observed with multidimensional imaging within 3 hours after excision. The direct comparison between non-linear images and histological images, although possible, is not always optimal, because the images arose from two different parts of the same sample.

2.3 Sample preparation

Histopathological samples were prepared according to standard methods (haematoxylin-and-eosin staining) and then imaged using a color digital camera connected to a common optical microscope. Non-conventional, axially cut histopathological samples were prepared following the standard method, but their slicing was performed with the skin surface parallel to the microtome blade. The non-conventional axially cut histology was performed only on selected samples, for which a previous histopathological diagnosis of BCC was already carried out. The margins were separately evaluated.

In multidimensional imaging, the sample was cut, maintaining both healthy skin and BCC, to obtain a regular shape, allowing its positioning with the skin surface either parallel to the optical axis (perpendicular optical sectioning), or orthogonal (en face optical sectioning). Before observation, the investigated samples were embedded in a 4% agarose gel to prevent unwanted movements during observation. A saline solution was used as immersion medium for the objective lens instead of water in order to maintain the natural osmolarity of the tissue.

2.4 Image acquisition and analysis

Excitation was accomplished using 120 fs width pulses at 90 MHz repetition rate, a wavelength of 740 nm for TPE and 840 nm for SHG and a mean laser power at the sample between 10 and 40 mW, depending on the depth of recording. These power levels are sufficiently low to avoid photobleaching and photodegradation effects, as demonstrated also in *in-vivo* multiphoton skin imaging [24]. Further, we verified that photodegradation starts at a power of about 60 mW at 70 μm below the skin surface (data not shown). SHG or TPE detection was accomplished by alternatively placing or removing a narrow band optical filter centered at half the excitation wavelength and by switching the excitation laser wavelength between 840 nm and 740 nm, respectively. TPE-SHG images were acquired with 512 × 512

#85395 - $15.00 USD Received 17 Jul 2007; revised 24 Jul 2007; accepted 24 Jul 2007; published 26 Jul 2007

pixels spatial resolution, from 100 μm to 250 μm lateral dimension, using a pixel dwell time of 5 μs. The scanning time was approximately 1.3 s for each image.

FLIM images were acquired with 256 × 256 pixels or 128 × 128 pixels spatial resolution, 200 μm lateral dimension and using a pixel dwell time of 200 μs. The scanning time was approximately 13.1 s for a 256 pixels image and 3.3 s for a 128 pixels image. Each FLIM image was acquired by scanning the same field of view twice. Measured photons detection times were allocated in a proportional address of a memory, with 64 time-channels for 256 pixels images and 256 time-channels for 128 pixels images. Instrument response function to a laser pulse was also measured in order to perform a proper de-convolution with the measured fluorescence decay curve. Image pixels exponential fits, image de-convolution and analysis were performed using the software SPC-Image 2.8 (Becker-Hickl GmbH, Berlin, Germany). The exponential decays of autofluorescence images were fitted using a single-exponential function. For ALA-treated samples an acquisition time of 40 to 80 s was used, and a three-exponential function was used as fitting function, in order to take into account both the slow and the fast lifetime components and to minimize the χ-square distribution. The parameter represented in the FLIM images was always the mean fluorescence lifetime. The mean value of a lifetime distribution corresponding to an image was evaluated, taking the standard error for the distribution as error.

MTPE images were acquired with 64 × 64 pixels spatial resolution, 150 μm lateral dimension, 16 spectral channels (13 nm each), using a pixel dwell time of 200 μs. The scanning time was approximately 0.83 s. Each image was acquired by scanning the same field of view eight times. The absorption and emission spectra were calculated summing the number of detected photons of each pixel over all the 64 time-channels and over the entire scanned image, and normalizing to the maximum value. The error of each spectral data point is typically the sum of the dark noise contribution and the statistical error corresponding to the photon counting. Since the dark noise contribution (10^{-2}) is one order of magnitude larger than the statistical error (10^{-3}), we neglected the last term, considering the dark noise the only source of uncertainty. The absorption spectra were evaluated in the same manner. They were normalized also to the square of the laser power. All the acquired spectra are corrected for the wavelength-dependent transmission of optics and detector sensitivity.

3. Results

The layered structure of human skin has been imaged using combined TPE and SHG microscopy on en face optically sectioned fresh samples. Images have been acquired at different depths ranging from 10 to 80μm. Unless histopathological comparison was performed, as in figure 1, it is difficult to identify the horny, granular, spinous or basal terms, because the BCC presence can alter the skin structure: the epidermis overlying BCC may be thinned, thickened or ulcerated, compared to normal skin. So in the following, when histopathological comparison is lacking, we will refer only to the depth of imaging.

In figures 1(a) and 1(c) (magnified detail), the epidermal layer is imaged at 50 μm depth, and was identified as the spinous layer by comparison with the corresponding histological section (Figs.1(b)). We suppose that this layer looks highly fluorescent because of its high concentration of keratins, as already demonstrated by Pena et al. [30]. There are several intrinsically fluorescent molecules inside skin, such as NADH, cholecalciferol, flavins, keratins, elastin, and also collagen. In a living cellular skin tissue, the main fluorescent contribution at Ti:SA laser excitation wavelengths is probably due to NADH and FAD molecules, involved in mitochondrial activity. In an ex-vivo tissue sample the NADH contribution vanishes and the main fluorescent emitter inside epidermis is keratin, while elastin and collagen are the main emitters inside dermis, as reported by Pena et al. [30]. Ours are ex-vivo fresh samples, imaged within 3-4 hours from excision. In this case we can probably appreciate both NADH and keratin contributions, since the NADH concentration is

#85395 - $15.00 USD Received 17 Jul 2007; revised 24 Jul 2007; accepted 24 Jul 2007; published 26 Jul 2007

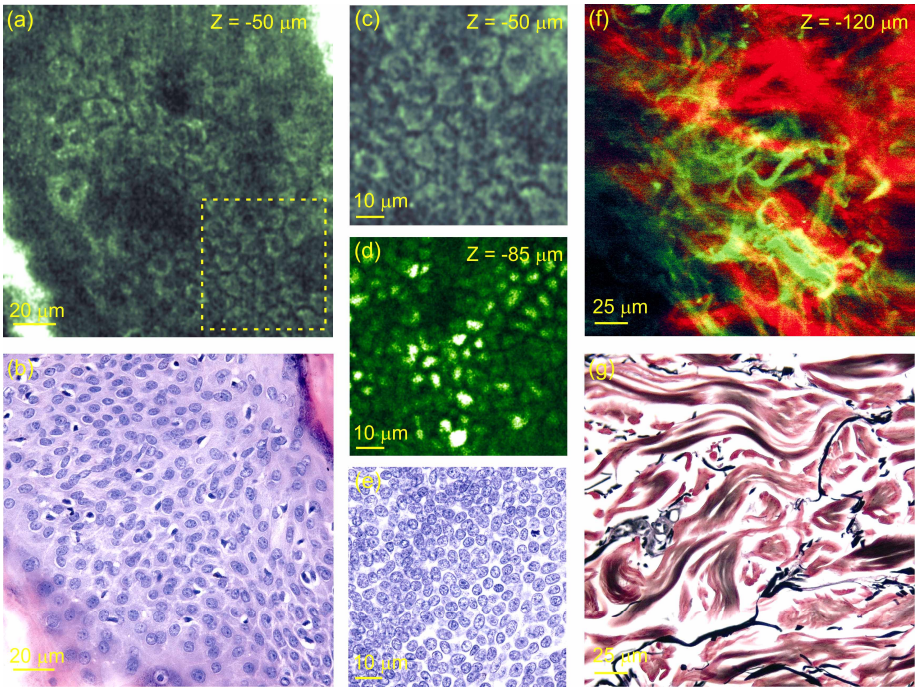

Fig. 1. Comparison between en face optically sectioned human skin sample imaged with combined TPE intrinsic fluorescence (green) and SHG (red) microscopy and corresponding microphotographs acquired with optical microscope on 5 µm thick axially sliced human skin samples stained with haematoxylin-eosin. TPE fluorescence image (a) and corresponding histology (b) at 50 µm depth, approximately corresponding to spinous layer. Field of view: 200 µm × 200 µm; scale bars: 20 µm. Magnified detail (corresponding to the dashed square in Fig. 1a) of healthy skin cells (c), acquired by TPE fluorescence. Field of view: 90 µm × 90 µm; scale bars: 10 µm. BCC cells in human skin at 85 µm depth acquired by TPE fluorescence (d) and corresponding histology (e). Field of view: 90 µm × 90 µm; scale bars: 10 µm. Elastic (green) and collagen (red) fibers in human skin at 120 µm depth acquired by combined TPE fluorescence and SHG (f) and corresponding histology stained with Verhoeff-Van Gieson stain (g). Field of view: 250 µm × 250 µm; scale bars: 25 µm. The excitation wavelength was 740 nm for TPE fluorescence and 840 nm for SHG.

still high enough to produce a detectable fluorescence signal. However, a confirmation of the high fluorescence signal from keratin is confirmed by the high signal detected from the first epidermal layer (data not shown), corresponding to the stratum corneum, which is composed of dead cells with high keratin concentration inside cellular membranes. In this image (Fig. 1(a)) cells are well resolved and appear with highly fluorescent cytoplasm and dark nuclei. BCC tissue (Figs. 1(d) and 1(e)) appears as a more homogeneous granular tissue with higher cellular density with respect to healthy skin cellular tissue. For the purpose of comparison, a magnified detail of healthy cells (corresponding to the dashed square in Fig. 1(a)) is represented in figure 1(c), with the same magnification used in Figs. 1(d) and 1(e).

Combined TPE-SHG imaging is a particularly powerful technique for dermis imaging. In Fig. 1(f) a TPE image of elastic fibers (in green) and a SHG image of collagen fibers (in red) of the same field are superimposed. Such image shows a good correlation with that obtained with a Verhoeff-Van Gieson stain on a formalin-fixed, paraffin-embedded normal skin sample (Fig. 1(g)). We selected the second harmonic generated signal by placing a narrow-band optical filter centered at exactly one-half the excitation wavelength in front of the detector. Further, we verified that the collected signal is only SHG by performing a measurement with spectral-lifetime detection (data not shown). Since SHG is a scattering process, the lifetime for SHG is

#85395 - $15.00 USD Received 17 Jul 2007; revised 24 Jul 2007; accepted 24 Jul 2007; published 26 Jul 2007

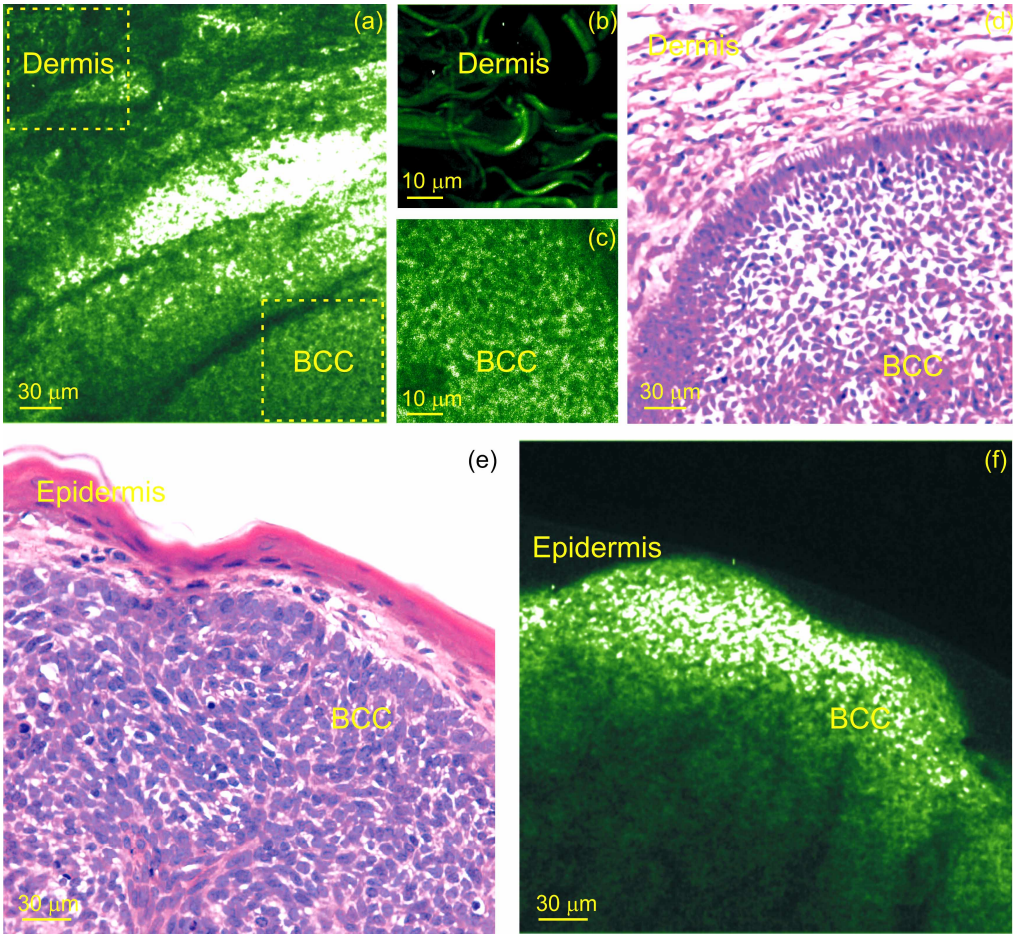

Fig. 2. Perpendicular optically sectioned human skin tissue image acquired using TPE autofluorescence on fresh sample, excised 4 hours after ALA application (a) and the corresponding microphotograph taken after conventional histological examination and visualization by optical microscope (d). Regions B and D are BCC tissue and healthy dermis, respectively. Field of view: 290 μm × 300 μm; scale bars: 30 μm. High magnified TPE autofluorescence images of healthy dermis (b) and BCC tissue (c), approximately corresponding to the regions B and D indicated in (a). Field of view: 90 μm × 90 μm; scale bars: 15 μm. Perpendicular optically sectioned human skin tissue imaged using TPE autofluorescence on fresh sample, excised 4 hours after ALA application (f) and corresponding histological microphotograph (e). Inside the sample both normal epidermis tissue E and BCC tissue B are present. Field of view: 300 μm × 300 μm; scale bars: 30 μm.

zero, whereas it is non-zero for fluorescence. The measurement we performed showed only a peak on very short lifetimes on the spectral channel centered at half the excitation wavelength, confirming that the signal collected from collagen is only SHG, without any fluorescence contribution.

Figures 1 were obtained by illuminating the sample with skin surface perpendicular to the excitation laser beam, equivalent to *in-vivo* imaging scheme. Figures 2 were instead obtained by illuminating the sample with the laser beam parallel to the skin surface. In this case, perpendicular optically sectioned samples can be directly compared to common histology. Figs. 2(a) (TPE imaging) and 2(d) (corresponding histological image) are both showing the dermis-BCC border. BCC tissue (B) and dermis tissue (D) are clearly distinguishable in regards to tissue morphology, as shown in the high-magnified images (Figs. 2(b) and 2(c)). BCC, with high cellular density, has a homogeneous granular structure; dermal tissue shows

#85395 - $15.00 USD Received 17 Jul 2007; revised 24 Jul 2007; accepted 24 Jul 2007; published 26 Jul 2007

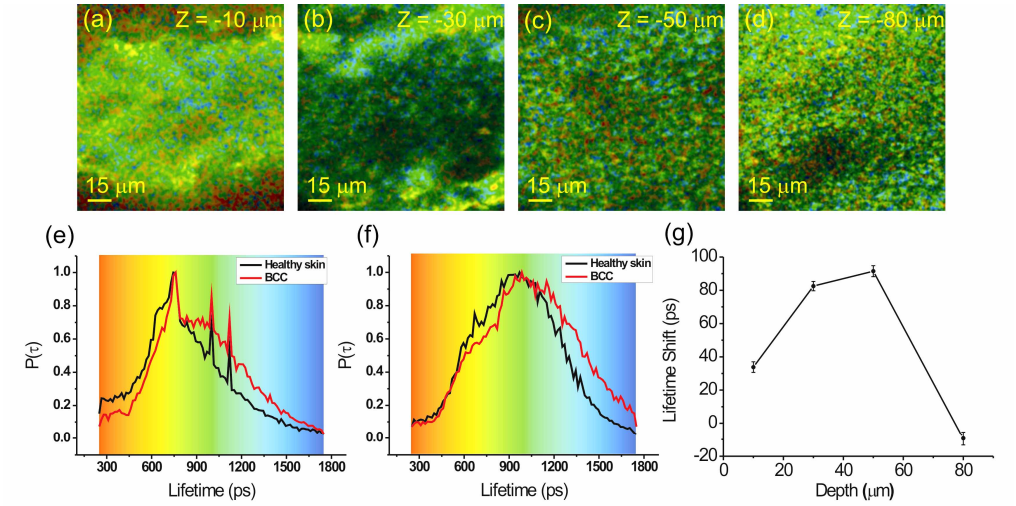

Fig. 3. FLIM images of an en face optically sectioned human healthy skin fresh sample, acquired by photon counting method, using an excitation wavelength of 740 nm. Image pixels lifetimes were obtained after system response de-convolution and single exponential fit and represented in a color-coded scale. Epidermal layers at 10(a), 30(b), 50(c), and 80(d) mm below the skin surface, respectively. Field of view: 130 µm × 130 µm; scale bars: 15 µm. The corresponding normalized lifetime distributions and the color-coded scale for 30 µm depth and 50 µm depth layers are plotted in (e) and (f) for healthy skin and BCC, respectively. The lifetime shift for each epidermal layer is plotted versus the depth of recording in (g).

large inhomogeneities and fibers (collagen and elastin). In some cases, we enhanced BCC autofluorescence by topical application of ALA to the lesion 4 hours before the excision. The topical application of ALA is useful in enhancing contrast when imaging skin tumor borders because of the selective accumulation of fluorescent protoporphyrine IX (PpIX) inside BCC tissue following the ALA application [37]. When ALA is applied, healthy epidermis tissue (E) is clearly discriminated from cancerous tissue (B) by the fluorescence light intensity (Fig. 2(f)), which is higher in BCC. The borders between normal and tumor tissue are well defined and the contrast is higher in the TPE image than in the corresponding histology (Fig. 2(e)).

In order to obtain useful data in perspective of a possible *in-vivo* imaging, we performed all the following measurements by coming back to the en face imaging illumination scheme (as in Figure 1). A layer-by-layer analysis using FLIM was performed in both healthy epidermis and BCC (Fig. 3). Fig. 3(a), 3(b), 3(c) and 3(d) show the lifetime images acquired inside healthy skin at a depth of 10, 30, 50, and 80 µm below the skin surface. Healthy tissue corresponding normalized mean lifetime distributions $P(\tau)$ of the image pixels are plotted in Figs. 3(e) and 3(f) for images acquired at 30 and 50 µm depth, (black line), respectively, together with the color-coded scale used. Compared to the normalized mean lifetime distributions of the images acquired at the same depths inside BCC tissue (red line), we observed a shift in the mean value. In particular, the mean lifetime distribution of healthy skin is shifted towards shorter values than BCC. The lifetime shift, plotted versus depth in Fig. 3(f), has a higher value in the intermediate epidermal layers, whereas it is reduced in the external layer and negligible in the deepest layer. In general, FLIM imaging shows a relatively small shift in lifetime between healthy skin and BCC. This shift has a value that is in general slightly higher than the biological variability of the samples. Even if further analysis, including a statistical analysis of a larger number of samples, would be suitable to draw more substantial conclusions, the multispectral analysis, as described below, showed a similar behaviour with evident spectral shifts between BCC and healthy skin in the intermediate layers.

#85395 - $15.00 USD Received 17 Jul 2007; revised 24 Jul 2007; accepted 24 Jul 2007; published 26 Jul 2007

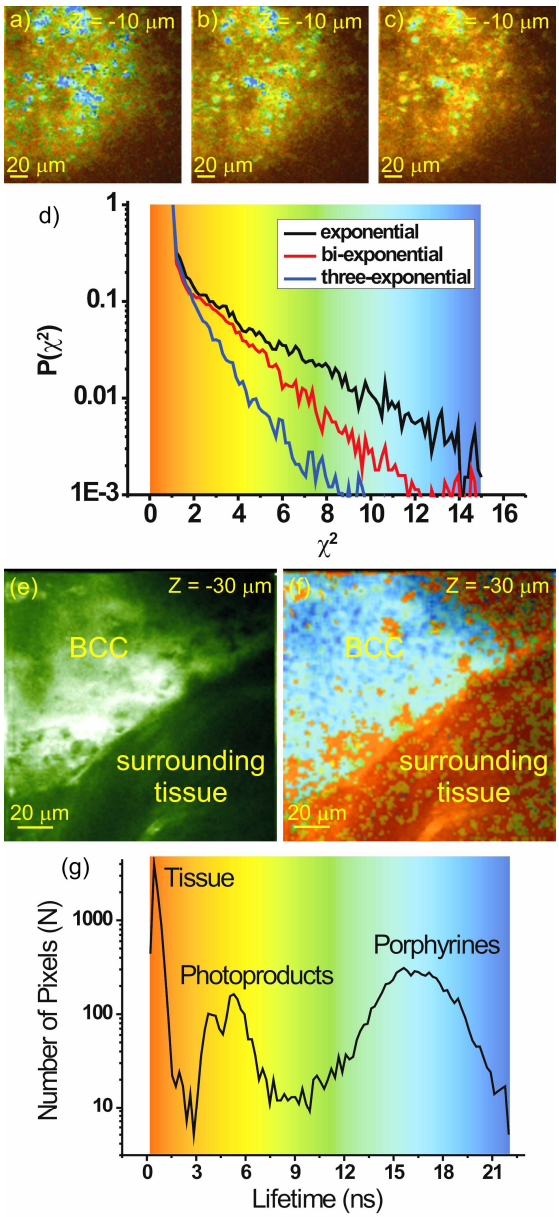

Fig. 4. χ-square color-coded matrixes for an image acquired by photon counting inside ALA-treated BCC tissue and fitted with a single-exponential (a), with a bi-exponential (b), and with a three-exponential (c) decay function. Field of view: 200 µm × 200 µm. Scale bars: 20 µm. χ-square distributions and color-coded scale (d) for the single-exponential (black line), the bi-exponential (red line), and the three-exponential (blue line) decay function, corresponding to the matrixes represented in (a), (b), and (c), respectively. En face optically sectioned human skin tissue image acquired using TPE autofluorescence on fresh sample, excised 4 hours after ALA application (e) with the corresponding high contrast FLIM image (f), obtained after system response de-convolution and three-exponential fit of the image pixels fluorescence decay. Inside the sample both normal healthy skin tissue (H) and BCC tissue (B) are present. Field of view: 200 µm × 200 µm; scale bars: 20 µm. The color-coded scale and the mean lifetime distribution of the image in (f) are plotted in (g) in a logarithmic scale.

#85395 - $15.00 USD Received 17 Jul 2007; revised 24 Jul 2007; accepted 24 Jul 2007; published 26 Jul 2007

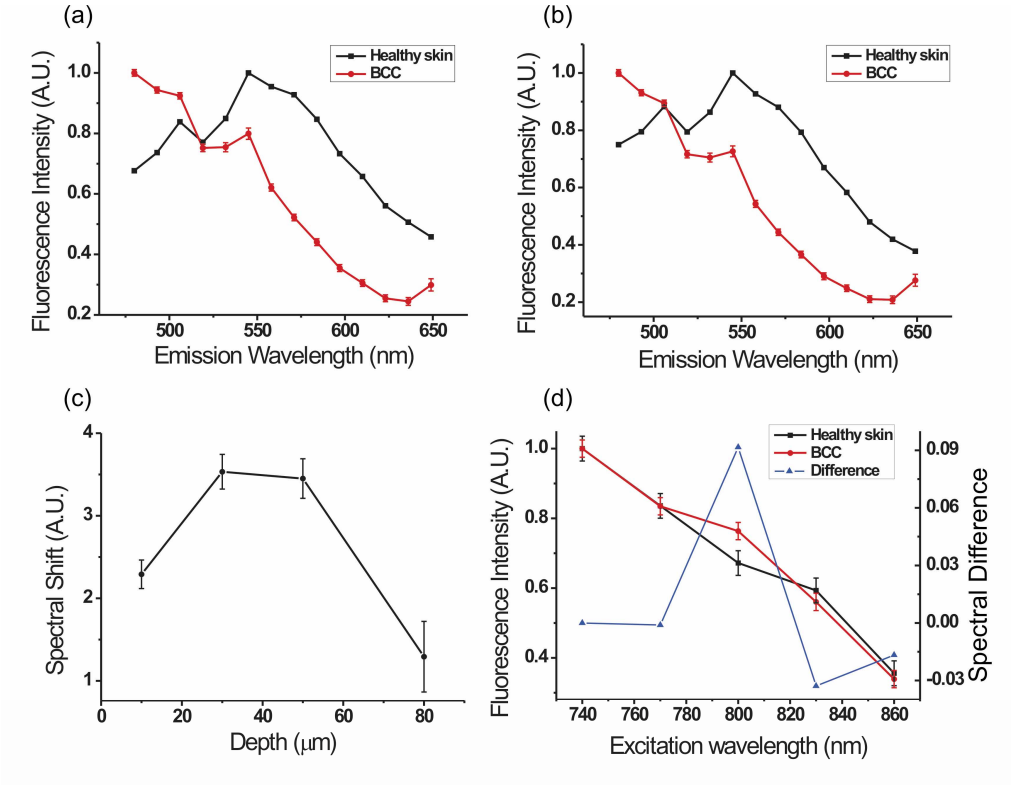

Fig. 5. Normalized TPE fluorescence emission spectra measured at 30 μm depth (a), and at 50 μm depth (b) below the skin surface for human healthy skin (black line) and BCC (red line) using 740 nm excitation wavelength. The "Spectral Shift" (calculated as the enclosed area between healthy skin and BCC fluorescence emission spectra) is plotted versus the depth of recording in (c). The normalized TPE fluorescence response varying the excitation wavelength is represented in (d) for a healthy skin cellular layer (black) and for a BCC cellular layer (red) as well as the difference between the two (blue).

ALA-treated samples were also imaged en face using FLIM. ALA application causes the accumulation inside tumor tissue of PpIX, having a longer fluorescence lifetime with respect to skin intrinsic fluorescent molecules. For this reason a multi-exponential fitting function was used in ALA-treated samples in order to take into account both the fast (corresponding to skin intrinsically fluorescent proteins) and the slow (corresponding to PpIX) lifetime components. Figs. 4(a), 4(b), and 4(c) show the χ-square matrixes obtained by fitting the fluorescence decays of an image acquired inside an ALA-treated BCC sample with a single-exponential, a bi-exponential and a three-exponential decay function, respectively. The corresponding χ-square distributions, together with the color-coded scale, are plotted on the graph in Fig. 4(d), confirming the presence of at least three different lifetime components. In fact, the χ-square distribution decreases with increasing the number of lifetime components. During the acquisition, we integrated collected photons for 40 to 80 s, in order to have a count value high enough to perform a three-exponential fit. We also performed binning of three adjacent pixels in the image, in order to obtain a maximum photon counting value of at least 10^4 in the most significant time channel. ALA-treated samples show not only enhanced fluorescence from BCC tissue, but also a large difference in lifetime distribution. A TPE image (Fig. 4(e)) confirms that BCC tissue (B) is more fluorescent than healthy skin (H). The corresponding FLIM image (Fig. 4(f)) reveals a higher contrast between healthy skin and BCC because of the accumulation inside BCC of PpIX, having a longer lifetime (more than 8 ns) with respect to skin tissue intrinsic fluorescent molecules (typically within 2 ns). This PpIX accumulation

#85395 - $15.00 USD Received 17 Jul 2007; revised 24 Jul 2007; accepted 24 Jul 2007; published 26 Jul 2007

is confirmed by the fluorescence lifetime distribution (Fig. 4(g)), which exhibits three peaks. The peak centered on the shortest lifetimes corresponds to the skin tissue intrinsic fluorescent molecules. The peak centered on the longest lifetimes is caused by the PpIX contribution. The peak in the middle is probably due to the presence of photoproducts and aggregates of PpIX. In fact, similar results have been found by Kress et al. [37] using single-photon fluorescence. We verified that the middle peak is not an artifact of the fitting software, by observing a similar lifetime distribution even using a double-exponential fitting function.

The layer-by-layer analysis was extended to MTPE imaging. The fluorescence emission of both healthy skin and BCC tissues was recorded in the 475-650 nm spectral range. In a first set of measurements we kept the excitation wavelength centered at 740 nm. Figs. 5(a) and 5(b) show the acquired fluorescence spectra for healthy skin (in black) and BCC (in red) at 30 and 50 μm depth, respectively. BCC emission spectrum is shifted towards shorter wavelengths with respect to healthy skin. The "Spectral Shift", defined as the normalized measure of the area enclosed between the healthy skin and the BCC emission spectra, is plotted versus depth in Fig. 5(c), showing that this quantity has a larger value in the intermediate layers than in the external ones, with a behavior similar to that shown by the lifetime shift results. A second set of measurements was performed varying the excitation wavelength in a 740-860 nm range. Fig. 5(d) shows the results obtained for BCC (red circles) and healthy skin (black squares) fluorescence response. The two spectra are quite similar at all the examined excitation wavelengths, except for the value at 800 nm where a higher fluorescence response was measured for BCC. The spectral difference (blue triangles), plotted versus the excitation wavelength on the same graph, always exhibits a module within the 4%, except at 800 nm (approximately 12%).

4. Discussion and conclusions

TPE imaging of the dermis showed an inhomogeneous appearance due to different types of fibers (collagen and elastic fibers) organized in a network, whereas BCC was clearly distinguished by aggregates of autofluorescent cells. Normal skin and tumor images obtained by TPE and SHG showed a close correlation with those obtained by conventional histopathology. The clear advantage of TPE-SHG compared to conventional histopathology is that it does not require the complex, invasive and somehow destructive sample preparation.

ALA is one of the most widely used photosensitizers in photodynamic therapy, which selectively induces PpIX accumulation inside epithelial tumors. By means of its large two photon action cross section, application of ALA resulted in an increased fluorescence emitted by tumor tissue. This effect is particularly helpful in enhancing contrast and in increasing penetration depth imaging capability, hence improving the ability to discriminate skin tumor borders by TPE fluorescence. The use of ALA could be extended to other epithelial skin tumors imaged by TPE and also to a directed biopsy or Mohs surgery.

Our study demonstrated that the use of ALA can be extended to FLIM imaging of skin tumors to increase the ability of discrimination between healthy skin and BCC . When combined with the application of ALA, FLIM allows higher contrast imaging of the skin lesion borders by means of the longer lifetime exhibited by PpIX, selectively accumulated in BCC tissue, with respect to skin tissue intrinsically fluorescent molecules. A longer fluorescence lifetime of PpIX has been already demonstrated in BCC and in different types of cells by using single photon fluorescence lifetime imaging [35,39]. However, many studies have to be performed to elucidate the time-dependence behavior of PpIX mean lifetime and the photoeffects caused by high-energy density pulsed illumination.

Even without ALA application, FLIM imaging was able to assess some differences between healthy skin and BCC. A lifetime shift between healthy skin and BCC was found in each tissue layer, by means of a fluorescence lifetime analysis. We found that healthy skin mean lifetime distribution is shifted towards smaller values with respect to the corresponding BCC distribution. The large shift (more than 80 ps) and the small shift (less than 20 ps) observed in the intermediate and in the external epidermis layers suggest that the differentiation between healthy skin and BCC occurs in the intermediate epidermal layers.

#85395 - $15.00 USD Received 17 Jul 2007; revised 24 Jul 2007; accepted 24 Jul 2007; published 26 Jul 2007

Nevertheless, the biological significance of this lifetime shift in autofluorescence images is not still completely understood. A possible cause could be a difference in the oxidative stress between healthy skin and BCC. In fact, it has been demonstrated that free NADH has a different fluorescence lifetime from that of bound NADH [40]. Thus, FLIM imaging may represent a method to measure the oxidative stress in living tissues [41], although NADH is not the only contributor to the detected autofluorescence. Our measured mean fluorescence lifetime is influenced by the presence of different fluorescent species, hence the observed lifetime shift may be due to a difference in relative concentration of fluorescent molecules between the two tissues, as well as a difference in the optical and electrical properties of the surrounding medium.

MTPE imaging showed a shift towards shorter wavelengths in the two photon emission spectrum between healthy skin and BCC: this spectral shift is likely to be caused by a different protein composition of the two tissues. Specifically, the spectral shift was evident in the intermediate layers, while it was minimal in the peripheral layers. These observations are in line with what has been found with FLIM technique and confirm that the differentiation between healthy skin and BCC occurs in the intermediate layers of the epidermis. By varying the excitation wavelength a larger two photon absorption for the BCC tissue at 800 nm wavelength was found, whereas a similar absorption spectrum was measured in the other spanned wavelengths (740-860 nm). At this wavelength there are several fluorescent molecules in skin, including NADH, riboflavins, folic acid, and cholecalciferol (vitamin D_3), which has a two photon absorption peak at 800 nm [4]. Vitamin D_3 is related to the growth of BCC and other carcinomas and its high concentration in BCC tissue has already been demonstrated using real time PCR and immunohistochemistry [42,43]. Hence, we can hypothesize that the observed absorption peak at 800 nm is due to an accumulation of Vitamin D_3 in BCC.

In conclusion, we have adopted a multidimensional imaging approach in morphological and spectroscopic characterization of BCC by combining most of non-linear laser microscopy techniques (TPE, SHG, FLIM, MTPE). Our multidimensional approach was able to characterize different tissue regions having different morpho-functional characteristics. In all the examined cases we obtained a good correlation with histopathology. Unfortunately, the comparison between corresponding non-linear and histological images is not perfect, because in general images arose from two adjacent parts of the same sample. However, all the histological features of the tissue can be determined in both non-linear and histological images, with a good, even if not optimal, correlation between them. However, we believe that this method at the moment is not intended as a diagnostic tool, but useful to prepare the in-vivo measurements. When in-vivo optical biopsy will be performed a comparison with histology will be mandatory. Also, a morphological, spectroscopic characterization and discrimination between different histotypes of BCC is beyond the scope of this article, even if our preliminary measurements have suggested that it is difficult to perform the discrimination by means of a morphological investigation (TPE-SHG).

It is worth noting that it is beyond the scope of this paper to test the diagnostic accuracy of this method in discriminating between BCC and healthy skin. This would require first of all a higher statistics, and can be demonstrated finally only by in-vivo measurements. Also, it should be investigated in the future how well FLIM and SHG are able to discriminate BCC from its mimics such as benign tricoblastic proliferations, trichoepithelioma or even chronic inflammation. However, the differential diagnosis between BCC and benign follicular adnexal neoplasms such as trichoepithelioma and trichoblastoma requires conventional histopathology and it cannot be based on multiphoton microscopy. Such differential diagnosis would be difficult also with the help of dermoscopy/epiluminescence microscopy or any other imaging technique applied to the skin. This would be anyhow beyond our aims. Our general aim is not to resolve such difficult differential diagnoses but rather to move from ex-vivo to in-vivo examination of skin tissues and to use multiphoton microscopy directly on the skin before biopsy and histological examination (so called optical biopsy) to provide clinicians with additional morphological information beyond clinical examination. In this view, we strongly

#85395 - $15.00 USD Received 17 Jul 2007; revised 24 Jul 2007; accepted 24 Jul 2007; published 26 Jul 2007

believe that one of the possible future applications of our method in vivo will be the recognition of BCC aggregates from chronic inflammation in the early recognition of BCC recurrences and identification of tumor margins.

Finally, we have demonstrated the use of ALA as a contrast agent in tumor borders detection with multidimensional non-linear imaging. The data obtained in this paper represent further support for *in-vivo* BCC non-invasive imaging and can be extended to other inflammatory and neoplastic skin conditions.

Acknowledgments

We thank European Laboratory for Non-linear Spectroscopy (Grant number TOK-MC-509761) and Ente Cassa di Risparmio di Firenze for financial support to this project and F. Vanzi for critical reading and comments.

#85395 - $15.00 USD Received 17 Jul 2007; revised 24 Jul 2007; accepted 24 Jul 2007; published 26 Jul 2007